MIC(0) preconditioning of 3D FEM problems on unstructured grids: Conforming and non-conforming elements

Svetozar Margenov *, Nikola Kosturski

Acad. G. Bonchev Street, bl. 25A, 1113 Sofia, Bulgaria

ARTICLE INFO

ABSTRACT

In this study, the topics of grid generation and FEM applications are studied together following their natural synergy. We consider the following three tetrahedral grid generators: NETGEN, TetGen, and Gmsh. After that, the performance of the MIC(0) preconditioned conjugate gradient (PCG) solver is analyzed for both conforming and non-conforming linear FEM problems. If positive off-diagonal entries appear in the corresponding matrix, a diagonal compensation is applied to get an auxiliary M-matrix allowing a stable MIC(0) factorization. The presented numerical experiments for elliptic and parabolic problems well illustrate the similar PCG convergence rate of the MIC(0) preconditioner for both, structured and unstructured grids.

© 2008 Elsevier B.V. All rights reserved.

1. Introduction

Mesh generation techniques are now widely employed in various scientific and engineering fields that make use of physical models based on partial differential equations. While there are many works devoted to finite element methods (FEM) and their applications, it appears that the issues of meshing technologies in this context are less investigated. Thus, in the best cases, this aspect is briefly mentioned as a technical point that is possibly non-trivial. In this study, the topics of grid generation and FEM applications are studied together following their natural synergy. This paper is a direct continuation of our recent study on two-dimensional grids [7].

Let $\Omega \subset \mathbb{R}^3$ be a bounded domain with boundary $\partial \Omega = \Gamma = \Gamma_D \cup \Gamma_N$, where $\Gamma_D \cap \Gamma_N = \emptyset$. The following elliptic (1) and parabolic (2) problems are considered:

$$
\begin{aligned}
-\nabla \cdot (a(\mathbf{x})\nabla u(\mathbf{x})) &= f(\mathbf{x}), \quad \mathbf{x} \in \Omega, \\
u(\mathbf{x}) &= u_D(\mathbf{x}), \quad \mathbf{x} \in \Gamma_D, \\
(a(\mathbf{x})\nabla u(\mathbf{x})) \cdot \mathbf{n} &= g_N(\mathbf{x}), \quad \mathbf{x} \in \Gamma_N,
\end{aligned}
\tag{1}
$$

$$
\begin{aligned}
\frac{\partial u(\mathbf{x}, t)}{\partial t} - \nabla \cdot (a(\mathbf{x}, t)\nabla u(\mathbf{x}, t)) &= f(\mathbf{x}, t), \quad (\mathbf{x}, t) \in \Omega \times [0, T], \\
u(\mathbf{x}, 0) &= u_0(\mathbf{x}), \quad \mathbf{x} \in \Omega, \\
u(\mathbf{x}, t) &= u_D(\mathbf{x}, t), \quad (\mathbf{x}, t) \in \Gamma_D \times [0, T], \\
(a(\mathbf{x}, t)\nabla u(\mathbf{x}, t)) \cdot \mathbf{n} &= g_N(\mathbf{x}, t), \quad (\mathbf{x}, t) \in \Gamma_N \times [0, T].
\end{aligned}
\tag{2}
$$

Let us introduce the triangulation $\mathcal{T}_h$ of Ω and the uniform mesh ω_τ with a time step $\tau > 0$ in $[0, T]$. The finite element method (FEM) associated with $\mathcal{T}_h$ and the FEM with Crank–Nicholson scheme on $\mathcal{T}_h \times \omega_\tau$ are used to discretize the problems (1) and (2) respectively. Then, the elliptic problem (1) is reduced to the system

$$
K\mathbf{u}_h = \mathbf{f}_h,
\tag{3}
$$

* Corresponding author.
  E-mail addresses: margenov@parallel.bas.bg (S. Margenov), kosturski@parallel.bas.bg (N. Kosturski).

where K stands for the stiffness matrix. At each Crank–Nicholson time step, the following linear system is to be solved

$$\left(M + \frac{\tau}{2}K\right)\mathbf{u}_h^{n+1} = \left(M - \frac{\tau}{2}K\right)\mathbf{u}_h^n + \tau \mathbf{f}_h^{n+\frac{1}{2}}, \tag{4}$$

where the upper index of the unknown vector indicates the number of the current time step, and M stands for the mass matrix. The modified incomplete Cholesky factorization MIC(0) is used in the preconditioned conjugate gradient (PCG) [2] solution of the systems (3) and (4).

The implementation of two variants of finite elements defined on $\mathcal{T}_h$ is studied, namely, conforming (Courant) and non-conforming (Crouzeix–Raviart) linear finite elements.

Each of these methods has its advantages and disadvantages when the problem is used in a particular application. The general assumption is that non-conforming elements are applied for problems where the lower order conforming elements are not robust.

For instance, in the case of highly heterogeneous media the non-conforming finite elements have proven to be accurate and locally conservative, see e.g. [1]. The non-conforming finite elements have also some advantages in the case of strongly coupled problems. For example, the projection schemes are currently among the most efficient ways to build a stable discretization of the initial-boundary value problem for the Navier–Stokes equations. Let us note that the Crouzeix–Raviart linear finite elements in a combination with piecewise constants provide *inf-sub* stable and computationally efficient discretization of the velocity–pressure fields. As a result, decoupled non-conforming FEM elliptic/parabolic problems are to be solved at the prediction step, see e.g. [3] and the references therein.

We investigate the following three grid generators: NETGEN, TetGen, and Gmsh. The presented qualitative analysis is based on the range of the dihedral angles of the triangulation for a given test domain. It is well known that very small and very large angles directly affect the accuracy of the FEM approximation. Such kind of strong mesh anisotropy deteriorates also the condition number of the related stiffness matrix, and as will be shown later on, the convergence rate of the implemented iterative solution methods. Some advantages of NETGEN are observed in this respect.

The remainder of the paper is organized as follows. Some needed background about MIC(0) factorization is given in the next section. Section 3 contains an analysis of the diagonal compensation. The comparison of the considered mesh generators is summarized in Section 4. Section 5 discusses some issues, related to the uniform refinement of unstructured tetrahedral grids. Numerical tests for structured (model) and unstructured (general) grids are presented in Section 6. Short concluding remarks are given at the end.

2. MIC(0) preconditioning

We recall some known facts about the modified incomplete Cholesky factorization MIC(0) [4,5]. Let $A = (a_{ij})$ be a symmetric $N \times N$ matrix and let

$$A = D - L - L^{\mathrm{T}}, \tag{5}$$

where D is the diagonal and $(-L)$ is the strictly lower triangular part of A. Then we consider the factorization

$$C_{\text{MIC(0)}} = (X - L)X^{-1}(X - L)^{\mathrm{T}}, \tag{6}$$

where $X = \text{diag}(x_1, \ldots, x_N)$ is a diagonal matrix, such that the sums of the rows of $C_{\text{MIC(0)}}$ and A are equal, i.e.,

$$C_{\text{MIC(0)}}\mathbf{e} = A\mathbf{e}, \qquad \mathbf{e}^{\mathrm{T}} = (1, \ldots, 1) \in \mathbb{R}^N. \tag{7}$$

Theorem 2.1. *Let $A = (a_{ij})$ be a symmetric $N \times N$ matrix and let*

$$L \geq 0, \tag{8}$$
$$A\mathbf{e} \geq 0, \tag{9}$$
$$A\mathbf{e} + L^{\mathrm{T}}\mathbf{e} > 0. \tag{10}$$

Then there exists a stable MIC(0) factorization of A, defined by the diagonal matrix $X = \text{diag}(x_1, \ldots, x_N)$, where

$$x_i = a_{ii} - \sum_{k=1}^{i-1} \frac{a_{ik}}{x_k} \sum_{j=k+1}^{N} a_{kj} > 0. \tag{11}$$

Remark 2.1. The numerical tests, presented in Section 6 are performed using the perturbed version of MIC(0) algorithm, where the incomplete factorization is applied to the matrix $\tilde{A} = A + \tilde{D}$. The diagonal perturbation $\tilde{D} = \tilde{D}(\xi) = \text{diag}(\tilde{d}_1, \ldots \tilde{d}_N)$ is defined as follows:

$$\tilde{d}_i = \begin{cases} \xi a_{ii} & \text{if } a_{ii} \geq 2w_i, \\ \xi^{1/2} a_{ii} & \text{if } a_{ii} < 2w_i, \end{cases}$$

where $0 < \xi < 1$ is a parameter and $w_i = \sum_{j>i} -a_{ij}$.
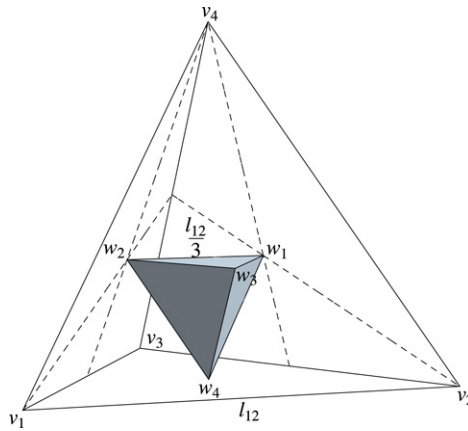
Fig. 1.　A Crouzeix–Raviart non-conforming linear element.

3. Diagonal compensation

It is known, that due to the positive off-diagonal entries of the stiffness matrix K, the MIC(0) factorization is not directly applicable to precondition the FEM system. The diagonal compensation is a simple general approach to avoid this problem.

3.1. Elliptic problems

The stiffness matrix K corresponds to a certain FEM discretization of the elliptic problem (1) on the triangulation $\mathcal{T}_h$. When there are some positive off-diagonal entries in the matrix, the stability condition (8) for the MIC(0) factorization is not satisfied. The diagonal compensation is the simplest procedure to approximate K by an M-matrix $\bar{K}$, in order to apply the MIC(0) factorization. This means that the positive off-diagonal entries of K are vanished, setting the diagonal of $\bar{K}$, such that the equal row sum condition is fulfilled, i.e., $K\mathbf{e} = \bar{K}\mathbf{e}$.

The standard FEM procedure of freezing the isotropic coefficient $a(\mathbf{x})$ on each finite element (the usual notation a_e for the element-wise integral mean value approximation of $a(\mathbf{x})$ will be used) leads to the consideration of a piecewise Laplacian problem. The global stiffness matrix reads as

$$K = \sum_{e \in \mathcal{T}_h} K_e, \tag{12}$$

where K_e is the current element stiffness matrix, and the summation sign stands for the FEM assembling procedure. When necessary we will use the notations $K^{(c)}$, $K_e^{(c)}$, $K^{(nc)}$, $K_e^{(nc)}$, where (c) and (nc) indicate the cases of conforming and non-conforming elements.

The following important geometric interpretation of the element stiffness matrix $K_e^{(c)}$ holds (see, e.g., in [8])

$$K_e^{(c)} = \frac{a_e}{6} \begin{bmatrix} \displaystyle\sum_{1 \neq i < j} l_{ij} \cot \theta_{ij} & -l_{34} \cot \theta_{34} & -l_{24} \cot \theta_{24} & -l_{23} \cot \theta_{23} \\ -l_{34} \cot \theta_{34} & \displaystyle\sum_{2 \neq i < j \neq 2} l_{ij} \cot \theta_{ij} & -l_{14} \cot \theta_{14} & -l_{13} \cot \theta_{13} \\ -l_{24} \cot \theta_{24} & -l_{14} \cot \theta_{14} & \displaystyle\sum_{3 \neq i < j \neq 3} l_{ij} \cot \theta_{ij} & -l_{12} \cot \theta_{12} \\ -l_{23} \cot \theta_{23} & -l_{13} \cot \theta_{13} & -l_{12} \cot \theta_{12} & \displaystyle\sum_{i < j \neq 4} l_{ij} \cot \theta_{ij} \end{bmatrix}, \tag{13}$$

where l_{ij} denotes the length of the edge connecting vertices v_i and v_j of the tetrahedron e, and θ_{ij} stands for the dihedral angle along this edge. This presentation shows that each positive off-diagonal entry in the element stiffness matrix corresponds to an obtuse dihedral angle in the tetrahedron e. The related positive entry tends to infinity when the dihedral angle tends to $180°$.

Now, let us turn on to the case of Crouzeix–Raviart non-conforming finite elements. The related test functions are piecewise linear with interpolation nodes at the centers of mass (centroids) of the faces of the tetrahedral element instead of the vertices (as is for the standard Courant elements). Let us denote with $\{w_i\}_{i=1}^4$ the centroids of the faces of the tetrahedron and with e^* the tetrahedral element associated with these vertices. Then, it is easily seen that the edges of the tetrahedron e^* are three times smaller than the edges in the original tetrahedron (see Fig. 1).

The basis functions of the non-conforming element are the same as the basis functions of the small conforming element e^*. If we denote these basis functions with $\{\varphi_i\}_{i=1}^4$, the element stiffness matrices can be written as

$$K_{e^*}^{(c)} = \left[\int_{e^*} a(\mathbf{x})\nabla\varphi_i \cdot \nabla\varphi_j\right]_{i,j=1}^4,$$

$$K_e^{(nc)} = \left[\int_e a(\mathbf{x})\nabla\varphi_i \cdot \nabla\varphi_j\right]_{i,j=1}^4,$$

and, since the volume of the tetrahedron e is 27 times larger than the volume of e^*, it follows that $K_e^{(nc)} = 27K_{e^*}^{(c)}$. Furthermore, from the geometric representation of the element stiffness matrix (13), it is easily seen that $K_e^{(c)} = 3K_{e^*}^{(c)}$. This leads to the next useful lemma.

Lemma 3.1. *Let us consider an arbitrary convex tetrahedron e. Then the following relation holds*

$$K_e^{(nc)} = 9K_e^{(c)}, \tag{14}$$

where $K_e^{(c)}$ and $K_e^{(nc)}$ stand for the related element stiffness matrices corresponding to linear conforming (Courant) and linear non-conforming (Crouzeix–Raviart) finite elements.

One direct conclusion from (14) is the applicability of the geometric interpretation (13) to the case of non-conforming linear tetrahedral elements.

Lemma 3.2. *Let us consider a piecewise Laplacian elliptic problem discretized by linear conforming finite elements on a tetrahedral mesh $\mathcal{T}_h$. Then, the stiffness matrix $K^{(c)}$ is an M matrix if all dihedral angles of $\mathcal{T}_h$ are smaller than or equal to $90°$.*

Lemma 3.3. *Let us consider a piecewise Laplacian elliptic problem discretized by linear non-conforming finite elements on a tetrahedral mesh $\mathcal{T}_h$. Then, the stiffness matrix $K^{(nc)}$ is an M matrix if and only if all dihedral angles of $\mathcal{T}_h$ are smaller than or equal to $90°$.*

Note that the condition that there are no obtuse dihedral angles in the mesh is sufficient in both cases and necessary only in the case of Crouzeix–Raviart finite elements.

It is observed, that the relative condition number $\kappa(\bar{K}^{-1}K)$ tends to infinity when the maximal dihedral angle tends to π. Since the MIC(0) factorization is applied to the auxiliary matrix $\bar{K}$, the convergence rate of the MIC(0)–PCG solver strongly deteriorates with the raise of dihedral angles in the FEM mesh.

In the two-dimensional (2D) case, the relative condition number of the diagonal compensation is known to be bounded by a constant depending on the minimal angle $\theta_{\min}$ of the triangulation only. The proof of the following sharp estimate

$$\kappa(\bar{K}^{-1}K) \leq \cot^2\theta_{\min}$$

can be found in our recent publication [6]. It is well known that the element stiffness matrix in the 2D case depends only on the triangle angles, and not on both the angles and the lengths of the edges, as is in the three-dimensional (3D) case. Moreover, the sum of the angles in the triangle is always fixed and the triangle can have at most one obtuse angle.

In the 3D case, there can be up to three obtuse dihedral angles in a single element. Moreover, we do not know any simple relation between the edge lengths and the dihedral angles in the tetrahedron. Thus, the 3D analysis of the relative condition number of the matrices K_e and $\bar{K}_e$ seems to be much more complicated than in the 2D case.

3.2. Parabolic problems

When the Crank–Nicholson scheme is implemented solving the parabolic problem (2) we have to get a preconditioner for the matrix $M + \frac{\tau}{2}K$. Then, the diagonal compensation for K in combination with lumping the mass for M are applied before the MIC(0) factorization. At this point, an advantage of the non-conforming Crouzeix–Raviart elements is, that the related mass matrix is always an M-matrix, i.e., lumping the mass is thus not required.

4. Comparison of mesh generators

In this section, we compare the following three mesh generators:

- NETGEN v.4.4 (http://www.hpfem.jku.at/netgen/);
- Tetgen v.1.4.1 (http://tetgen.berlios.de/);
- Gmsh v.2.0.0 (http://geuz.org/gmsh/).
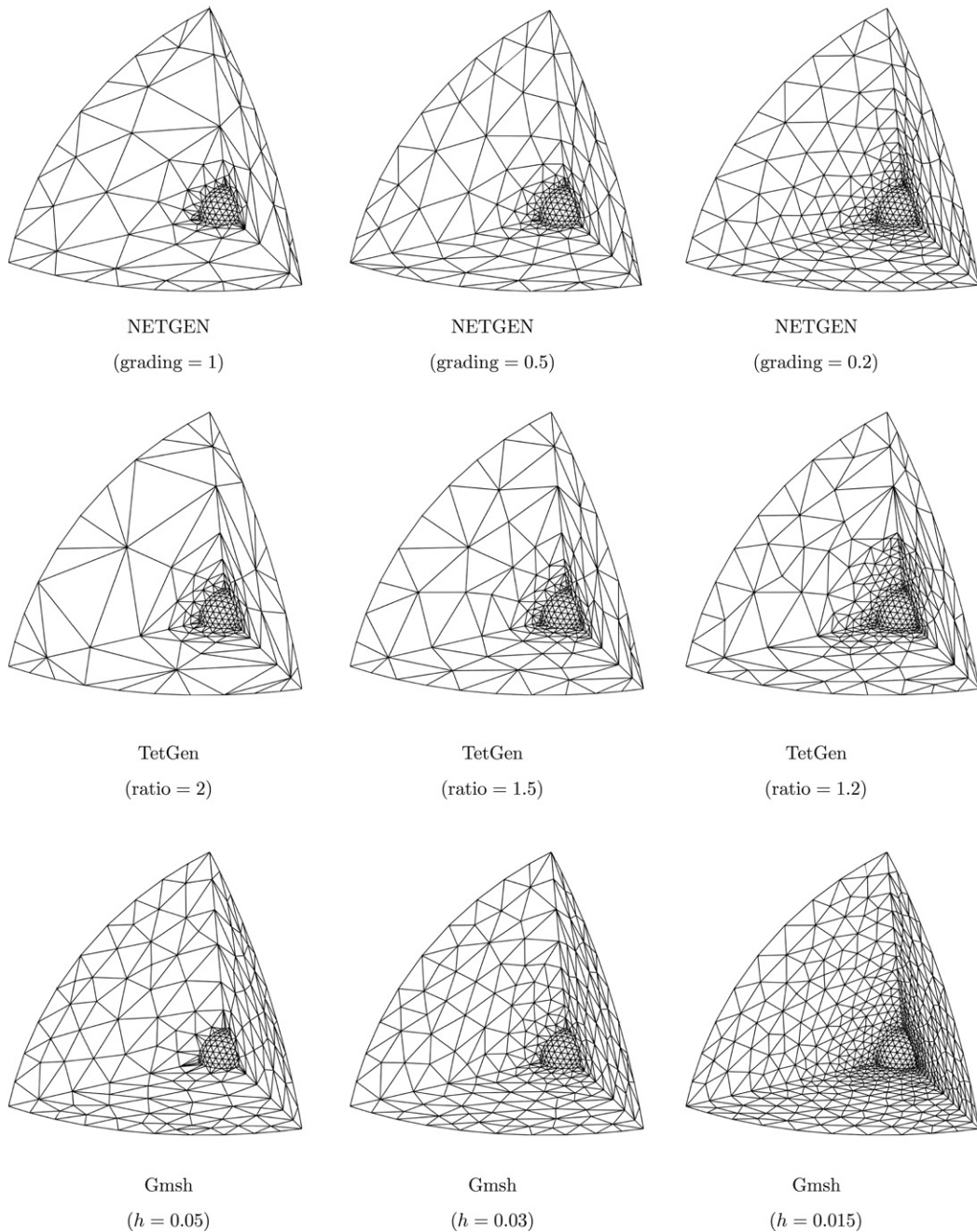
Fig. 2. Test meshes, generated by the three considered generators with different settings.

As was already mentioned, the appearance of very small and very large angles in the FEM mesh, strongly deteriorates the accuracy of the numerical solution and the condition number of the related stiffness matrix. In the previous section we also paid a special attention on the negative impact of the large dihedral angles on the MIC(0)–PCG convergence rate.

The domain we chose for the presented comparative analysis is

$$\Omega = \{(x, y, z) \mid 0.1 \leq x^2 + y^2 + z^2 \leq 1, x, y, z \geq 0\}. \tag{15}$$

Different parameters of the grid generators may affect the quality of the resulting meshes. Some generated meshes are shown in Fig. 2. The obtained minimal and maximal angles, and the related number of nodes and elements are given in Table 1.

The mesh quality of NETGEN highly depends on the *mesh-size grading* parameter. Decreasing the value of this parameter leads to meshes with better dihedral angles at the expense of larger number of elements and nodes.

Table 1
Properties of the resulting test meshes

Generator	Parameters	Min. angle (°)	Max. angle (°)	Elements	Nodes
NETGEN	Grading = 1	14.3553	151.997	436	189
NETGEN	Grading = 0.5	19.3608	142.821	650	245
NETGEN	Grading = 0.2	26.1134	135.173	1882	504
TetGen	Ratio = 2	5.06703	166.432	474	197
TetGen	Ratio = 1.5	6.26918	169.619	714	251
TetGen	Ratio = 1.2	6.12442	168.717	1484	417
Gmsh	$h = 0.05, H = 0.5$	13.3345	143.297	1192	344
Gmsh	$h = 0.03, H = 0.3$	20.9614	144.173	1553	436
Gmsh	$h = 0.015, H = 0.15$	18.7442	137.373	3718	940
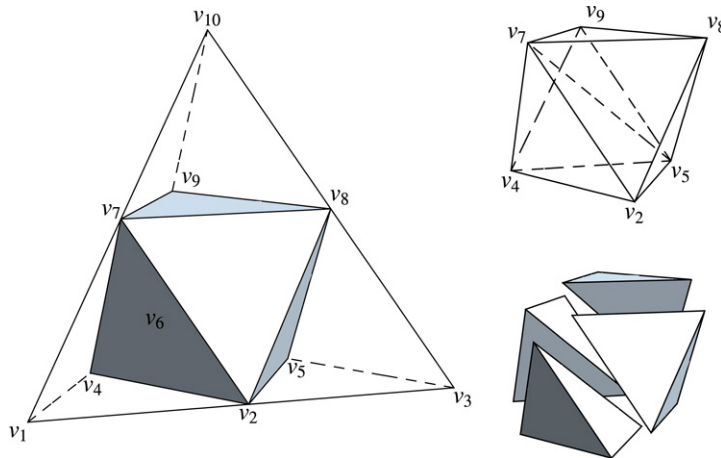
Fig. 3. Tetrahedron subdivision into eight parts.

In TetGen, the mesh element quality criterion is based on the *minimum radius–edge ratio*, which limits the ratio between the radius of the circumsphere of the tetrahedron and the shortest edge length. It seems, however, that this parameter does not directly reflect on the dihedral angles. For all tested values, the resulting meshes contain both very small and very large dihedral angles.

For Gmsh, the parameters h and H correspond to the *characteristic lengths*, assigned respectively to the vertices on the inner and the outer spherical boundary of the domain.

The presented results show that NETGEN generally achieves better dihedral angles than TetGen. Similar dihedral angles are obtained with Gmsh, but due to considerably larger number of elements/nodes, than with NETGEN.

5. Mesh refinement

In 2D case, the uniform refinement of a triangular mesh is simply defined by splitting of each triangle to four, connecting the midpoints of the sides. The resulting triangles are similar to the original one, preserving the angles of the coarser triangulation. Unfortunately, a completely similar statement does not hold in 3D case.

One 3D uniform splitting is shown in Fig. 3. First, four tetrahedra, similar to the original one, are cut from the corners (see the left part of the figure). After that, the remaining octahedron is split to four parts. This splitting involves selecting a diagonal. The diagonal $v_5 v_7$ is chosen here (see the top right part of the figure). Usually, the shortest of the three diagonals should be chosen to obtain the best result. The bottom right part of the figure shows the corresponding tetrahedral splitting of the octahedron.

It is important to note, that this uniform refinement could substantially deteriorate the angles of the triangulation. Let us consider, for example, the platonic tetrahedron with equal dihedral angles $\theta = \cos^{-1}(\frac{1}{3}) \approx 70.5288°$. After one step of uniform refinement, the tetrahedra that are part of the related octahedron have dihedral angles ranging from $\frac{1}{2}\cos^{-1}(-\frac{1}{3}) \approx 54.7356°$ to $\cos^{-1}(-\frac{1}{3}) \approx 109.471°$.

The good news is, that the consequent uniform refinement does not generate a further increase of the mesh anisotropy. The octahedron is split to six similar octahedra, and eight tetrahedra similar to the original one. The same procedure is applied recursively, preserving the angles obtained at the first refinement step.

NETGEN provides a *volume optimization* operation. Table 2 shows the properties of some meshes, obtained by consecutive refinement steps via volume optimization. The starting (coarsest) mesh is the best one from the previous section (see NETGEN with grading = 0.2 in Table 1).

Table 2
Refined meshes

Mesh	Min. angle (°)	Max. angle (°)	Elements	Nodes
1	26.1134	135.173	1 882	504
2	16.1153	139.000	13 953	3 022
3	16.1153	135.846	107 530	20 589
4	16.1153	147.272	843 040	150 934
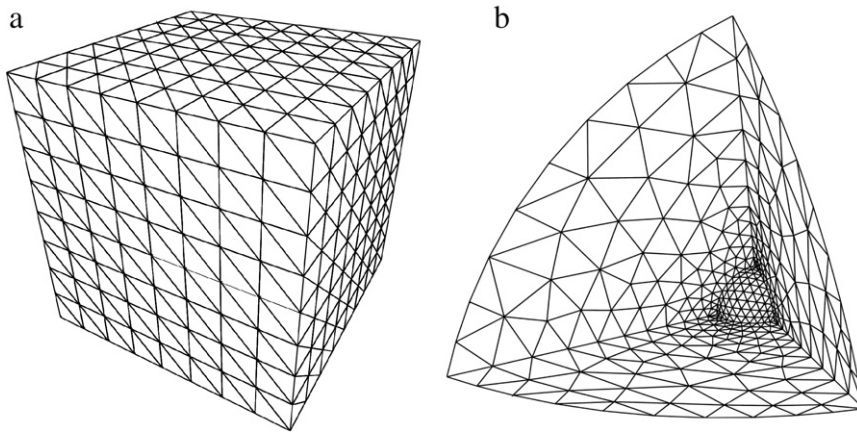
Fig. 4. Coarser structured (a) and unstructured (b) meshes, used in the numerical experiments.

These meshes are used in the next section to benchmark the MIC(0)–PCG solver for elliptic and parabolic problems on unstructured meshes.

6. Numerical experiments

The presented numerical tests illustrate the MIC(0)–PCG convergence rate. A relative PCG stopping criteria in the form $\mathbf{r}_k^T C^{-1} \mathbf{r}_k \leq \varepsilon^2 \mathbf{r}_0^T C^{-1} \mathbf{r}_0$ is employed. Here $\mathbf{r}_k$ is the residual vector at the kth iteration and C is the MIC(0) preconditioner. We compare the obtained results in the cases of linear conforming and non-conforming finite elements.

The considered model elliptic problem is

$$-\Delta u = f, \qquad \Gamma_D \equiv \partial \Omega, \tag{16}$$

with Dirichlet boundary conditions on the whole boundary corresponding to the exact solution

$$u(x, y, z) = x^3 + y^2 + z^4 + \sin(x - y).$$

The related parabolic problem is

$$\frac{\partial u}{\partial t} - \Delta u = f, \qquad \Gamma_D \equiv \partial \Omega, \tag{17}$$

where $t \in [0, 1]$, the time step is $\tau = 0.01$, and the Dirichlet boundary conditions on the whole boundary correspond to the exact solution

$$u(x, y, z, t) = x^4 + y^3 + \sin(x - z) + t^2.$$

Both (16) and (17) are solved on both structured and unstructured grids (see Fig. 4). Two types of finite elements are used to discretize the two model problems: conforming (Courant) and non-conforming (Crouzeix–Raviart).

The obtained iteration counts are presented in both table and graphic form. When parabolic problems are considered, the iteration count is the total number for all time steps. The asymptotic behavior of the MIC(0)–PCG solver is well expressed in all cases.

Remark 6.1. In the case of unstructured meshes, a generalized coordinate-wise ordering is used to ensure the conditions for a stable MIC(0) factorization.

Table 3
MIC(0)–PCG iterations for the model problems in the unit cube: Conforming FEM, $\varepsilon = 10^{-6}$

Mesh	Elements	Nodes	Elliptic	Parabolic
2	3 072	729	11	514
3	24 576	4 913	16	711
4	196 608	35 937	23	916
5	1 572 864	274 625	34	1127

Table 4
MIC(0)–PCG iterations for the model problems in the unit cube: Non-conforming FEM, $\varepsilon = 10^{-6}$

Mesh	Elements	Nodes	Elliptic	Parabolic
1	384	864	23	1108
2	3 072	6 528	31	1547
3	24 576	50 688	43	2267
4	196 608	399 360	61	3155
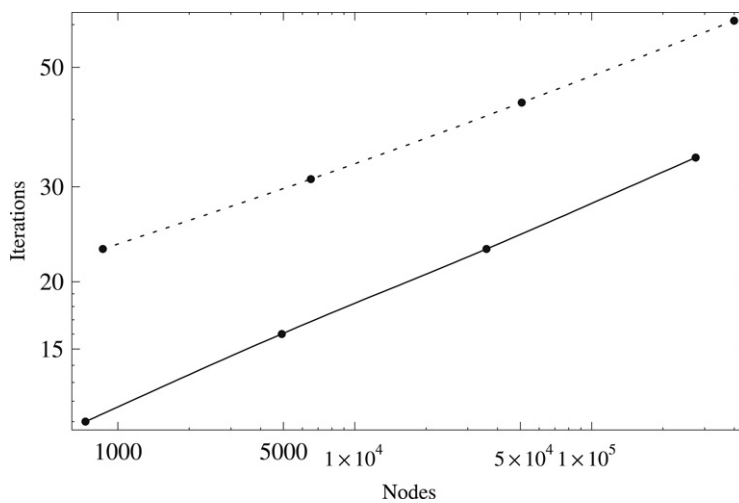
Fig. 5. Number of iterations for the elliptic model problem in the unit cube.

Table 5
MIC(0)–PCG iterations for the model problems in the curvilinear domain: Conforming FEM, $\varepsilon = 10^{-6}$

Mesh	Elements	Nodes	Elliptic	Parabolic
2	13 953	3 022	10	704
3	107 530	20 589	14	1007
4	843 040	150 934	20	1505

6.1. Structured grids

The results for the model problems on the unit cube with uniform structured grids are presented in Tables 3 and 4. They contain the number of iterations for conforming and non-conforming elements respectively.

The convergence rates are graphically presented in Figs. 5 and 6. The solid and dashed lines correspond to the cases of conforming and non-conforming finite elements. The plots give a better opportunity to compare the increase of the iteration counts with the size of the problem. The logarithmic scale more transparently illustrates the asymptotic behavior of the number of iterations.

6.2. Unstructured grids

The presentation in this section strictly follows the introduced setting from the previous one. Tables 5 and 6 and Figs. 7 and 8 contain the numerical results for the elliptic and parabolic test problems on the related unstructured grids.
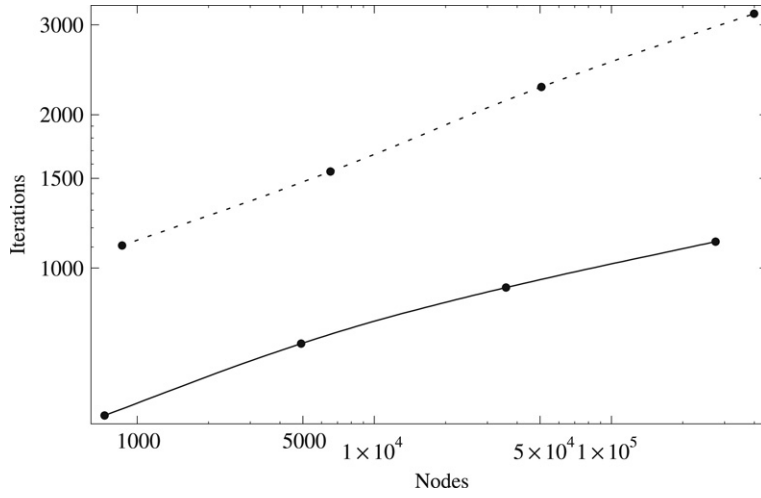
Fig. 6. Number of iterations for the parabolic model problem in the unit cube.
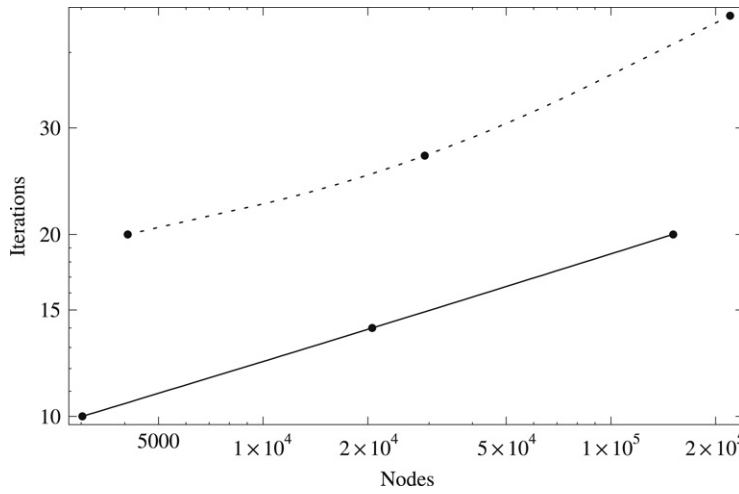
Fig. 7. Number of iterations for the elliptic problem in the curvilinear domain.
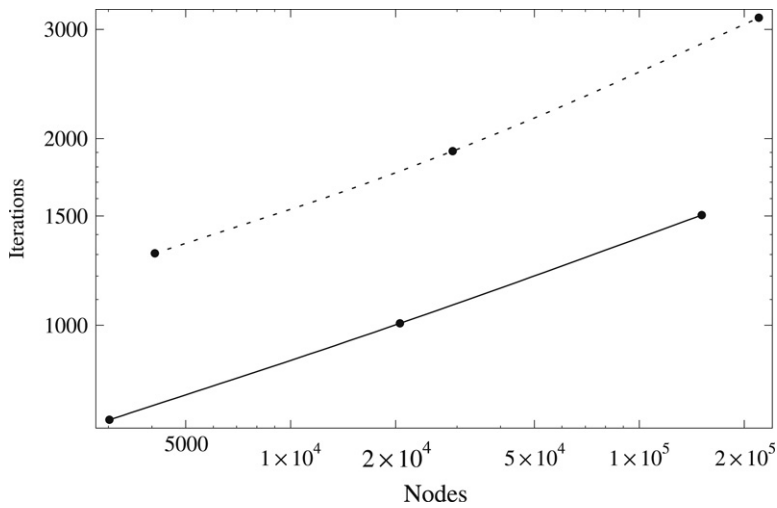
Fig. 8. Number of iterations for the parabolic problem in the curvilinear domain.

Table 6
MIC(0)–PCG iterations for the model problems in the curvilinear domain: Non-conforming FEM, $\varepsilon = 10^{-6}$

Mesh	Elements	Nodes	Elliptic	Parabolic
1	1 882	4 080	20	1306
2	13 953	29 170	27	1909
3	107 530	220 116	46	3132

6.3. Concluding remarks

The rigorous theory of MIC(0) preconditioning is directly applicable only to the model elliptic problem in the unit cube, discretized by standard linear conforming finite elements. For this simplest case, the reported number of iterations fully confirms the estimate $n_{it} = O(N^{1/6})$. Here, we observe the same asymptotic behavior of the PCG iterations for all remaining problems, which are not supported by the theory up to now, including the case of Crouzeix–Raviart non-conforming finite elements. As we see, the considered algorithms have a well-expressed stable behavior for the considered unstructured meshes. The next general conclusion is that the iteration count is smaller for the conforming FEM problems when compared to the results for non-conforming FEM systems of the same size. However, the stable convergence rate of the MIC(0)–PCG solver for Crouzeix–Raviart FEM systems is of a particular importance, due to the special robustness properties of these non-conforming elements.

Acknowledgment

References

[1] D.N. Arnold, F. Brezzi, Mixed and nonconforming finite element methods: Implementation, postprocessing and error estimates, RAIRO Model. Math. Anal. Numer. 19 (1985) 7–32.
[2] O. Axelsson, Iterative Solution Methods, Cambridge University Press, Cambridge, MA, 1994.
[3] B. Bejanov, J.-L. Guermond, P. Minev, A locally *div*-free projection scheme for incompressible flows based on non-conforming finite elements, Int. J. Numer. Meth. Fluids 49 (2005) 239–258.
[4] R. Blaheta, Displacement decomposition — incomplete factorization preconditioning techniques for linear elasticity problems, Numer. Linear Algebra Appl. 1 (1994) 107–126.
[5] I. Gustafsson, An incomplete factorization preconditioning method based on modification of element matrices, BIT 36 (1) (1996) 86–100.
[6] N. Kosturski, S. Margenov, Comparative Analysis of Mesh Generators and MIC(0) Preconditioning of FEM Elasticity Systems, Numerical Methods and Applications 2006, in: Springer LNCS, vol. 4310, 2007, pp. 74–81.
[7] N. Kosturski, S. Margenov, MIC(0) preconditioning of conforming and non-conforming fem problems on unstructured grids, in: Proc. SIMONA, 2006, pp. 78–87.
[8] J. Shewchuk, What Is a good linear finite element? — Interpolation, conditioning, anisotropy, and quality measures, in: Eleventh International Meshing Roundtable, 2002, pp. 115–126.